Latin American Journal of Solids and Structures
www.lajss.org

Dynamic Properties of High Volume Fly Ash Nanosilica (HVFANS) Concrete Subjected to Combined Effect of High Strain Rate and Temperature

Abstract
The study aims to determine the dynamic properties of high volume fly ash nanosilica (HVFANS) concrete exposed to strain rates between 30.12 to 101.42 s^{-1} and temperatures of 25, 400, and 700 ^{o}C by using split Hopkinson pressure bar (SHPB) machine. The static and dynamic compressive strengths of HVFANS concrete were slightly lower than plain concrete (PC) at room temperature, while its values were higher at 400 and 700 ^{o}C. The results proved that the CEB model of dynamic increase factor is more reliable to estimate the behaviour of HVFANS concrete at studied temperatures. The toughness, critical strain, and damage of HVFANS concrete recorded a superior performance than PC under studied strain rates and temperatures that would reflect the possibility of use HVFANS concrete in structures to improve its resistant of fire and impact loads, as well as to decrease the demand on Portland cement which could lead to restrict the risks of liberated gases during cement production. Furthermore, equations were proposed to estimate the dynamic increase factor, toughness, and critical strain of both concretes under investigated conditions.

Keywords
HVFA concrete; Nanosilica; DIF; SHPB; toughness; critical damage.

Mohamed H. Mussa[1*]
Azrul A. Mutalib[1]
Roszilah Hamid[1]
Sudharshan N. Raman[2]

[1]Department of Civil and Structural Engineering, Universiti Kebangsaan Malaysia, 43600 UKM Bangi, Selangor, Malaysia

[2]Department of Architecture, Universiti Kebangsaan Malaysia, 43600 UKM Bangi, Selangor, Malaysia

*eng.mhmussa@siswa.ukm.edu.my
azrulaam@ukm.edu.my
roszilah@ukm.edu.my
snraman@gmail.com

http://dx.doi.org/10.1590/1679-78254900

Received: February 04, 2018
In Revised Form: February 26, 2018
Accepted: March 11, 2018
Available online: March 20, 2018

1. INTRODUCTION

Since early decades of 20th century, numerous studies were conducted to assess the concrete properties under elevated temperature to ensure the safety of engineering structures [1-3]. The extensive use of high strength concrete (HSC) in modern construction motivated several scholars to study its thermal properties. The results were contradictory and indicated that the strength of HSC might deteriorate a higher or lesser than normal strength concrete (NSC) at elevated temperature [4-7]. Recently, several alternatives binders were widely used in HSC as a partial cement replacement to reduce the risks of CO_2 emissions liberated during cement production [8].

Fly ash (FA) was broadly utilized as a Portland cement replacement owing to it's a great performance in concrete and low price. FA is a by-product of the pulverized coal ignition in thermal power plants. Since the 1980s, high volume fly ash (HVFA) concrete started to use in Canada via replacing the Portland cement by 55 to 60% of FA [9]. There is no a unified definition for HVFA concrete until now. Sivasundaram et al. [10] stated that replacement of Portland cement with 30% of FA may define as HVFA concrete. However, other standards and researchers declared that FA replacement percentage should be above 40 or 50% [11-15].

The main disadvantage of using HVFA in concrete is decreasing of compressive strength at early ages due to the slow pozzolanic reaction of FA [16-20]. Hence, nanosilica (NS) were extensively used in HVFA concrete due to its high pozzolanic reactivity with CH liberated from cement hydration to produce calcium silicate hydrate (CSH) which greatly enhances the concrete strength [21-24]. Several studies were carried out on HVFA concrete with NS to investigate its thermal properties. Ibrahim [25, 26] reported that HVFANS concrete can be used as a fire proof material under temperatures reach up to 700 ^{o}C via replacing the Portland cement by 2.5 and 52.5% of NS and FA, respectively. Whereas the HVFANS concrete maintained about 94.54% of its room compressive strength after exposing to a temperature of 700 ^{o}C. In the same context, Radzi [27] used the same above proposed mixture of

(cc) BY

HVFANS concrete to fabricate a slab with dimensions of (1850 × 1700 × 200) mm and tested under temperature of 1100°C. The results revealed that the residual compressive strength was 62.2% of the original compressive strength at room temperature. Moreover, the temperatures of concrete cover and bottom reinforcement were less than 300°C with a maximum spalling depth and coverage area of 23 mm and 34.3%, respectively. It can be noted that these studies on HVFANS concrete were conducted under static load condition. However, the knowledge about the dynamic behaviour of this concrete at high strain rates and elevated temperatures has not been determined.

Several engineering structures such as tunnels and high-rise buildings might expose to an explosion by terrorist attacks during the service time such as the detonations of Moscow Metro in 2004, London Subway in 2005, and New York World Trade Centre in 2001 [28, 29]. These incidents and others highlighted a fact that concrete material of structures might be in danger of fire and blast loads simultaneously. The blast or impact loading usually results in a high strain rate effect on the construction material of structures, whereas fire causes a high temperature effect. These effects might cause a great change in the mechanical behaviour of concrete [3]. Therefore, understanding of HVFANS concrete behaviour under various conditions will increase the confidence of its application in the engineering sector.

The Split Hopkinson Pressure Bar (SHPB) machine was broadly used to study the dynamic properties of concrete and other materials under strain rates of 10 to 10^4 s^{-1} [30, 31]. Several studies utilized this machine to determine the properties of different concrete types subjected to the coupling effect of elevated temperature and high strain rate. Li [3] determined the dynamic properties of HSC concrete contained 4.5% of silica fume and 23% of FA under temperatures of 25, 200, 400, 600, and 800 ^oC. The results revealed that the dynamic compressive strength improved with the increase of strain rate and evidently decreased after a temperature of 400 ^oC. In addition, the dynamic increase factor (DIF) was increased linearly with the strain rate. Huo [32] studied the dynamic properties of NSC under elevated temperatures reach up to 700 ^oC. The outcomes indicated that the temperature and strain rate remarkably affected the dynamic increase factor (DIF) of concrete. Moreover, the residual dynamic strength of concrete evidently decreased with the increase of temperature, nevertheless, a clear influence of the temperature and strain rate did not observe on the shape of normalized stress-strain curves. Ziyan et al. [33] evaluated the dynamic behaviour of NSC concrete at temperatures of 25, 400, 600 and 800 ^oC under strain rate range of 30 s^{-1} to 220 s^{-1}. The results proved that the compressive strength of heated concrete was highly degradation as compared with concrete at ambient temperature. In addition, the effect of high temperature on the dynamic properties of concrete was more notable than that of strain rate.

He et al. [34] stated that NSC concrete under high temperatures and blast loads tended to be more sensitive to strain rate with the increase of high temperature. The dynamic properties of concrete at room temperature was clearly different from that at elevated temperatures more than 200 ^oC. Su et al. [35] demonstrated that the dynamic compressive strength of NSC increased by nearly 14% at a temperature of 400 ^oC as compared to the ambient temperature. Chen [36] studied the dynamic properties of NSC at elevated temperature reach up to 950 ^oC. The experimental results appeared that the dynamic compressive strength and stress-strain curve at elevated temperature still experienced remarkable strain rate effects. Moreover, the failure modes of rapidly loaded specimens at elevated temperatures were considerably different from those at room temperature. Zhai [37] studied the effects of strain rate ranged between 10^{-4} to 300 s^{-1} on NSC under elevated temperature reach up to 1000 ^oC. The results proved that the DIF of NSC after exposing to the elevated temperatures of 600 to 800 ^oC still appeared a close relationship with strain rate.

From the previous studies, it can be concluded that the fire and strain rate had notable effects on the dynamic strength of any type of concrete. Therefore, the mutual effects of elevated temperature and high strain rate on the mechanical behaviour of HVFANS concrete was evaluated. The recommended mixture proportion by Ibrahim [25, 26] was used to fabricate the HVFANS concrete samples due to its excellent thermal properties. The dynamic properties of HVFANS concrete were determined at temperatures of 25, 400 and 700 ^oC by using SHPB machine under average strain rate between 30.12 to 101.42 s^{-1} and the obtained results were compared with the plain concrete (PC).

2. EXPERIMENTAL TEST PROCEDURE

2.1 Materials of Concrete Mixture

Portland cement (Type I) manufactured based on Malaysian standard (MS 522) used in the concrete mixture [38]. The fly ash (FA) was collected from the Jimah power plant located at Malaysian Port Dickson and categorized as class F based on British standard (BS EN 450: 2005) [39]. The chemical compositions of Portland cement and FA were shown in Table 1.

Table 1. *Chemical compositions of Portland cement and fly ash.*

Items	Clinker %	Cement %	Fly ash %
SiO_2	21.66	21.28	44.16
Al_2O_3	5.8	5.6	24.6
Fe_2O_3	3.68	3.36	12.5
CaO	65.19	64.64	5.34
Mgo	2.86	2.06	2.5
TiO_2	-	-	4.1
K_2O	-	-	1.5
SO_3	0.2	2.14	0.3
Total alkalis	0.07	0.05	-
Insoluble residue	0.1	0.22	-
Loss of ignition, LOI	0.27	0.64	5

Table 2 showed the properties of colloidal nanosilica (NS) type Cembinder W8 provided by AkzoNobel Company, which was used in the concrete mixture to improve the early compressive strength of concrete that contained a high volume of FA.

Table 2. *Properties of colloidal nanosilica material.*

Surface area (m^2/g)	Average size (nm)	Silica concentration (%)	Bulk density (kg/m^3)	pH
80	35	50	1050	10

The fine aggregate was natural river sand passed through a 4.75 mm sieve size with a fineness modulus of 2.98 and bulk specific gravity of 2.53 [40, 41]. The loose and compacted bulk density of fine aggregate were 1510.18 and 1721.83 kg/m^3, respectively [42]. The coarse aggregate was crushed granite provided from local sources with a maximum size of 10 mm and bulk specific gravity of 2.07.

Superplasticiser (SP) type Darex Super 20 was utilized to acquire the desired workability of concrete mixture and increase the compressive strength by decreasing the required volume of mixing water based on naphthalene sulphonate. Fibrillated polypropylene (PP) fibres manufactured by Timuran Company with a length of 12 mm and specific gravity of 0.9 had utilized to increase the ductility of concrete and eliminate the surface spalling [43-47]. The dosage of SP was equal to 1% of cementitious materials weight and PP was equal to 1 kg/m^3 of concrete volume.

2.2 Mixture Preparation and Curing Process

American concrete institute standard (ACI 211.4R-93) [48] was applied to select the mixture proportions of PC and HVFANS concrete samples with water to cementitious materials ratio (w/c+p) equal to 0.29 and targeted static compressive strength of 60 MPa as shown in Table 3. The HVFANS concrete samples were prepared via replacing the cement with 52.5% of FA and 2.5% of NS based on the recommendations of Ibrahim's study conducted in Universiti Kebangsaan Malaysia (UKM) [25, 26].

Table 3. *Mixture materials (kg/m^3) of PC and HVFANS concrete.*

Concrete type	Cement	Sand	Gravel	Water	Sp	PP	FA	NS
PC	531.30	780.06	942.64	170.16	5.31	1	-	-
HVFANS	225.80	682.01	942.64	154.85	5.31	1	278.93	26.56

During the study, the serving sequence of materials according to ASTM C192 [49] caused cement balls particularly for HVFANS concrete because the mixture was quite hot and stiff. To avoid this problem, the fine and a portion of coarse aggregate with cement and FA were firstly mixed via horizontal pan mixer. Then, the colloidal NS and water were added to the mixture taking into consideration the water content of NS particles. Finally, the rest of coarse aggregate and PP were added to break up any noodles of the mixture [50]. The slump test was performed before adding SP and kept between 25 to 50 mm. The mixture was cast into cylindrical and cubic steel moulds with dimensions of (50 × Ø50) mm and (150 × 150 × 150) mm, respectively. The samples were de-moulded after 24 h,

except the HVFANS concrete specimens which stayed in moulds for 48 h [26]. Then, all the samples were placed into a water tank and cured for 28 days.

2.3 Heating Process

The static and dynamic properties of PC and HVFANS concrete samples were determined at high temperatures of 400 and 700 ^{o}C, these temperatures were selected according to prior studies performed by Ibrahim [25, 26]. The heating process followed ISO 834 fire curve [51] and carried out by using an electric furnace with the capacity of 3 concrete cubes and heating rate of 9 ^{o}C/min. After 2h of heating at the mentioned target temperatures, the heating process was stopped and then the samples were removed and cooled down to the ambient temperature.

2.4 Static Test

The static test was performed based on British standard (BS EN 12390-3) [52] by using an automatic compression test machine produced by Unit Test Scientific Company (UTS) with a loading capacity of 5000 kN. The average compressive strength values of the three specimens were recorded under 25, 400 and 700 ^{o}C at curing age of 28 days.

2.5 Dynamic Test

The dynamic test was conducted by using split Hopkinson pressure bar (SHPB) machine available in UKM laboratory as shown in Fig.1a and 1b [53, 54]. The SHPB machine consisted of striker bar moving inside launcher cylinder, incident bar and transmitter bar. All the bars are fabricated from stainless steel with Young modulus of 210 GPa and wave velocity of 5190 m/s. The bars designed with a large ratio of length to diameter in order to ensure uniaxial wave propagation through the bars. The bar diameter of 50 mm was found to be the most appropriate to achieve the minimum friction between bars and supports to reduce the waves dispersion which significantly improved the recorded signals of strain gauges as shown in Fig. 1c [53]. A good contact between bars and concrete samples was achieved to minimize friction by smoothing the sample surface with a hand grinder and sandpaper. In addition, the bars were well coaxial by using laser alignment within an accuracy up to 0.01 mm to satisfy the force equilibrium condition as shown in Fig. 1d [53].

A total of 150 cylindrical concrete samples with (50 × Ø50) mm were tested within an average of five samples for each applied strain rate under different thermal conditions for PC and HVFANS concrete. Lindholm [55] stated that the samples have to be short enough to rapidly achieve a uniform stress state along the length of concrete sample during loading. However, using of very short samples may lead to increase the friction between the bars and sample ends, hence an apparent rise in strength could occur [56]. The specimen diameter also requires to be small comparative to the wavelength of the applied load pulse to successfully achieve the theory of one dimensional wave without the complication of Pochhammer- Chree radial oscillations [57]. In most cases, the optimum ratio of length to diameter (L/D) is 0.5 according to the relationship suggested by Davies and Hunter [57] to prevent wave dispersion. Nevertheless, the experimental results of Davies and Hunter did not observe any obvious effect of specimen size on stress–strain curves within L/D ratios range between 0.31 to 1.55 [57]. Consequently, the L/D ratio was chosen to be 1 by using specimens with diameter of 50 mm and length of 50 mm. Similar L/D ratio was used by other researchers [53, 54].

During the test, the cylindrical concrete sample is sandwiched between the incident and transmitter bars, and then the striker bar was launched at a known velocity toward the incident bar to achieve the desired strain rate. Newton's second law applied to determine the striker's acceleration according to the pressure exerted on the striker bar [58, 59]. A compression stress pulse was generated into the incident bar during the impact and travelled in a uniaxial direction toward the interface between the incident bar and concrete specimen. Its amplitude mainly relied on the striker bar velocity [60, 61]. At this point, a part of the pulse is reflected back along the incident bar as a tensile pulse, and the remaining part is transmitted from the concrete sample to the transmitter bar as a compressive pulse and then recorded by a strain gauge.

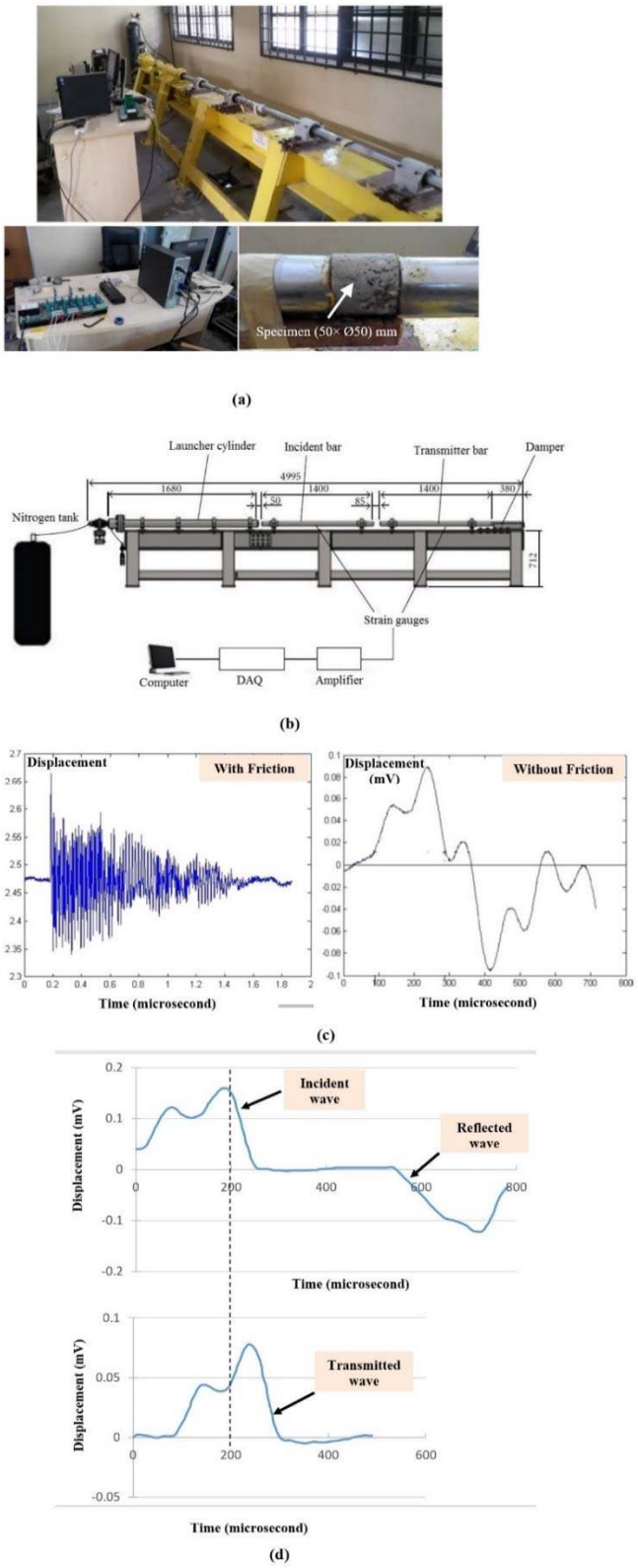


Fig. 1. *(a) SHPB machine view (b) Components of SHPB (mm) (c) Friction effect on incident wave (d) Recorded signals of incident and transmitted bars during the test*

Two Omega strain gauges' model (SGD-3/350-LY11) were used to mimic the material elongation of incident and transmitter bars. The change in the resistance of strain gauge was too small due to the low values of strain and the only way to detect its change is by using a voltage measurement. Therefore, the strain gauge was quarterly connected to Omega bridge sensors model (OM2-163) which considers as a complete signal conditioning system and consist of high performance instrumentation amplifier. The bridge sensors were connected to Omega data

acquisition module (OMB-DAQ-3000) which used (OMB-DaqView-XL) computer software to convert the analogy voltage signals to digital data that could be stored and analysed. MATLAB software was used to analyse the digital data and obtained the stress-strain diagrams of concrete samples. The strain gauge of the incident bar recorded the incident pulse $\varepsilon_i(t)$ and reflected pulse $\varepsilon_r(t)$, while the strain gauge on the transmitter bar measured the transmitted pulse $\varepsilon_t(t)$ [62]. Once all the pulses are recorded, the stress $\sigma(t)$, strain rate $\dot{\varepsilon}$(t), and strain $\varepsilon(t)$ histories of the sample can be computed, respectively, by using the following equations [54, 62, 63]:

$$\sigma(t) = \frac{AE}{2A_s}\left[\varepsilon_i(t) + \varepsilon_r(t) + \varepsilon_t(t)\right] \quad (1)$$

$$\dot{\varepsilon}(t) = \frac{C_0}{L_s}\left[\varepsilon_i(t) - \varepsilon_r(t) - \varepsilon_t(t)\right] \quad (2)$$

$$\varepsilon(t) = \frac{C_0}{L_s}\int_0^t \left[\varepsilon_i(t) - \varepsilon_r(t) - \varepsilon_t(t)\right] dt \quad (3)$$

where A, E, C_0 are the cross-sectional area, the Young's modulus and the wave velocity of the bar material, and, L_s, A_s are the length and cross-sectional area of the specimen.

3. RESULTS AND DISCUSSIONS

3.1 Static Test Results

Table 4 and Figure 2 indicated that the compressive strength of HVFANS concrete at room temperature was marginally decreased by 4.21% as compared with PC due to the high quantity of fly ash (FA) class F which contained a low amount of cement-like properties (CaO) [64]. HVFANS concrete appeared a clear increase in compressive strength at exposing temperature of 400 °C because the heating process significantly enhances the NS reactivity as well as increase the hydration process via producing a high-density calcium silicate hydrate structure which greatly improves the concrete strength [64].

Table 4. *Static compressive strength of PC and HVFANS concrete at various temperatures.*

Sample No.	Temperature (°C)					
	25		400		700	
	PC	HVFANS	PC	HVFANS	PC	HVFANS
1	62.66	57.95	58.61	67.79	38.87	51.6
2	59.08	61.55	56.48	61.01	33.54	52.13
3	61.82	56.68	59.48	64.86	36.71	46.26
Average (MPa)	61.19	58.72	58.19	64.55	36.37	49.99
Maximum Relative Error (%)	3.43	4.82	2.94	5.48	7.78	7.46

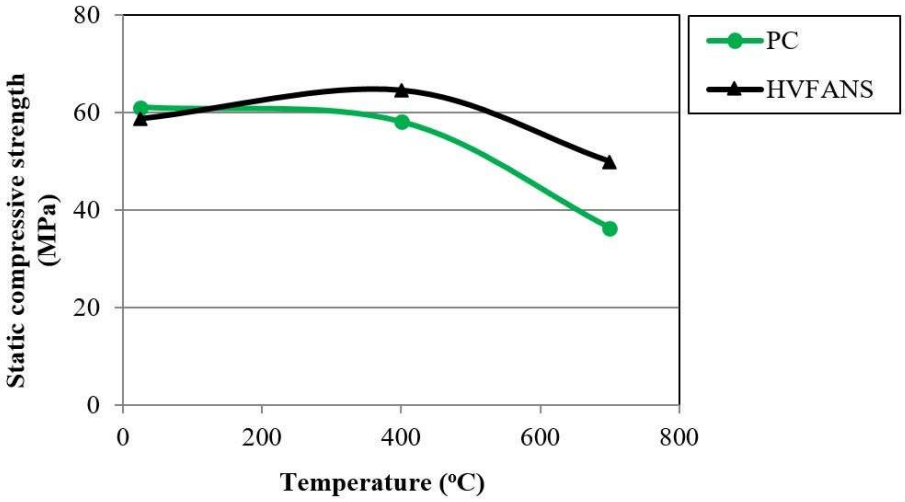


***Fig. 2**. Behaviour of PC and HVFANS concrete at different temperatures*

At temperature of 700 °C, a dramatic reduction in compressive strength of HVFANS and PC concrete was observed due to the extreme accumulation of vapour pressure inside the specimens which caused a large number of cracks, besides the dehydrate of cement paste binder products at this temperature. Nevertheless, HVFANS concrete revealed a higher residual compressive strength by 85.13% from their original strength at room temperature as compared with PC which maintained only 59.44%, this behaviour may attribute to the filler effect of NS in the mixture which increased the calcium silica hydrate content for HVFANS concrete. The relative error of each compressive strength group was less than 7.78% which revealed that the experimental records were fairly reliable.

3.2 Dynamic Test Results

3.2.1 Compressive Strength and dynamic increase factor (DIF)

The ultimate dynamic compressive strength represents the peak stress determined from stress-strain curves of PC and HVFANS concrete specimens subjected to five average strain rates and temperatures of 25, 400, and 700 °C as shown in Fig. 3.

The dynamic stress-strain curves appeared a close relationship with the increasing of average strain rate for both concrete types and the descending part of curves was pointed to the samples destruction and strain relaxing after ultimate stress [65]. The dynamic compressive strength increased approximately linearly with the increase of average strain rate for both concrete types under temperatures of 25, 400, and 700 °C as shown in Fig. 4.

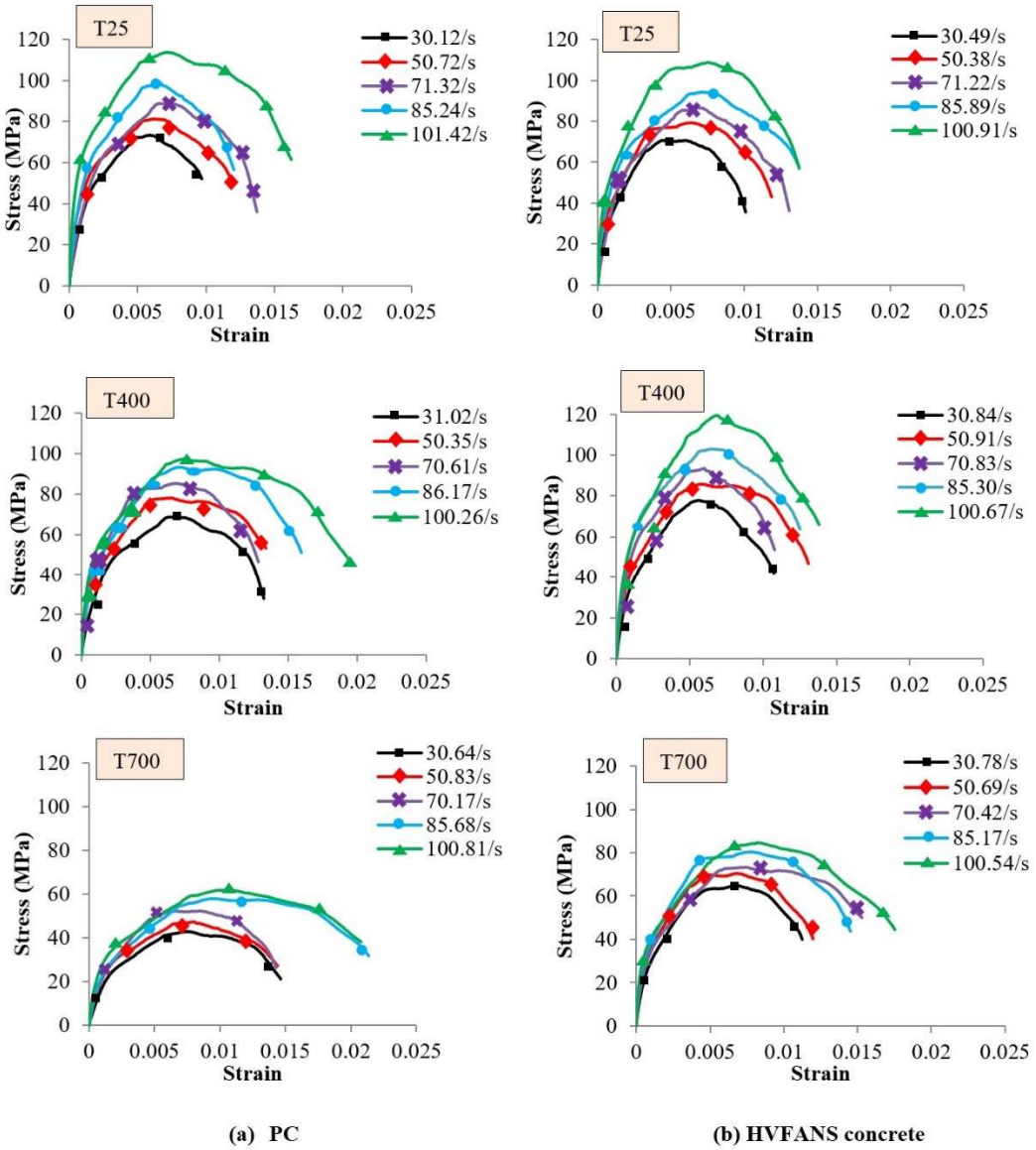


Fig. 3. *Stress-strain curves of PC and HVFANS concrete at various temperatures.*

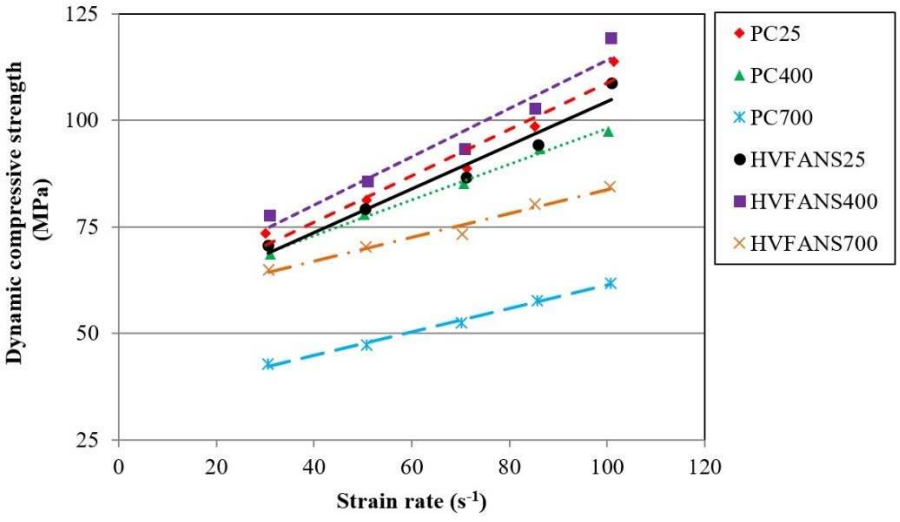


Fig. 4. *Dynamic compressive strength of PC and HVFANS concrete at different strain rates and temperatures.*

Small variations in compressive strength were observed at 400 °C for both concrete types; however, a rapid reduction was detected at 700 °C particularly for PC samples. The HVFANS concrete showed a good resistant for dynamic loads at exposing temperatures of 400 and 700 °C than PC in all the investigated cases of strain rate, that reflected the great effect of NS on concrete strength which works as a filler for small voids that may increase the calcium silica hydrate content in mixture.

Dynamic increase factor (DIF) broadly used to evaluate the effect of strain rate on the compressive strength and defined as the ratio between dynamic to static compressive strength [3, 34]. The results proved that DIF mainly depended on the strain rate and increased almost linearly with the increase of strain rate for PC and HVFANS concrete samples at all the investigated temperatures as shown in Fig. 5.

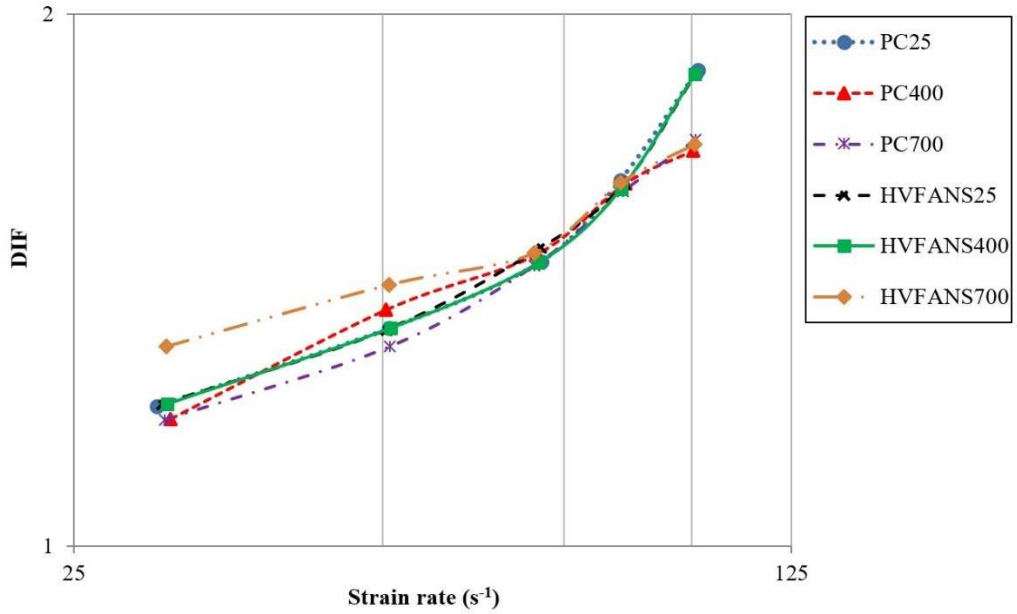


Fig. 5. *DIF of PC and HVFANS concrete at various strain rates and temperatures.*

The response surface methodology (RSM) available in the Design Expert Software (version 11) [66] was used for the statistical design and analysis of experimental data. The main goal was to derive an equation that could significantly represent the relationship of DIF with the exposing temperature (T) and dynamic strain rate ($\dot{\varepsilon}_d$). The linear and 2FI solver models with the inverse transformation were the most accurate to fit the experimental data of DIF for PC and HVFANS concrete, respectively, as follows:

For PC:

$$\frac{1}{DIF} = 0.943249 + 0.000028\ \mathrm{T} - 0.003796\ \dot{\varepsilon}_d \tag{4}$$

For HVFANS concrete:

$$\frac{1}{DIF} = 0.980249 - 0.000156\ \mathrm{T} - 0.004310\ \dot{\varepsilon}_d + 2.08303*10^{-6}*T*\dot{\varepsilon}_d \tag{5}$$

where: T is the exposing temperature between 25 to 700 °C, and $\dot{\varepsilon}_d$ is the dynamic strain rate within a range of 30.12 to 101.42 s^{-1}.

The results of variance analysis (ANOVA) were used to evaluate the accuracy of the adopted models as shown in Table 5. The outcomes revealed that the current models can be efficiently used to predict the values of DIF for both types of concrete within the mentioned ranges of temperature and strain rate. The quality of the fit polynomial model was expressed by the value of correlation coefficient (R^2) which should be close to 1 with a minimum value of 0.8 [67, 68]. Moreover, the differences between "Predicted R^2" and "Adjusted R^2" should be less than 0.2 and the Adequate Precision (AP) which measures the signal to noise ratio of the models should be greater than 4 [69].

Table 5. *The results of ANOVA analysis for DIF models of PC and HVFANS concrete.*

Concrete	Transformation	Model	R^2	Adjusted R^2	Predicted R^2	Adequate Precision (AP)
PC	inverse	linear	0.9826	0.9797	0.9736	45.6237
HVFANS	inverse	2FI	0.9764	0.9700	0.9516	35.9775

Several experimental tests had extensively used the DIF to evaluate the effects of dynamic strain rate on concrete in tension or compression [70, 71]. Based on to their studies, expressions were recommended to determine the DIF of concrete in compression as follows:

a) In the 1993s, CEB [72] proposed an equation to calculate the DIF of concrete in compression under high strain rates reach up to 300 s^{-1}:

$$DIF_{CEB} = \begin{cases} \left(\dot{\varepsilon}_d / \dot{\varepsilon}_s\right)^{1.026\alpha_s} & For\ \dot{\varepsilon}_d \le 30\, s^{-1} \\ \gamma_s \left(\dot{\varepsilon}_d / \dot{\varepsilon}_s\right)^{1/3} & For\ \dot{\varepsilon}_d > 30\, s^{-1} \end{cases} \quad (6)$$

where $\dot{\varepsilon}_d$ is dynamic strain rate, $\dot{\varepsilon}_s$ is static strain rate which equal to $30 \times 10^{-6}\ s^{-1}$, $\alpha_s = 1/(5 + 9\, f_{cs}/10)$, $\log \gamma_s = 6.156\alpha - 2$, and f_{cs} is static compressive strength in MPa.

b) In the 1997s, Tedesco et al. [73] derived an equation to determine the DIF of concrete, whereas the transition from low strain to high strain rates was occurred at 63.1 s^{-1}:

$$DIF_{Tedesco} = \begin{cases} 0.000965 \log \dot{\varepsilon}_d + 1.058 & For\ \dot{\varepsilon}_d \le 63.1\ s^{-1} \\ 0.758 \log \dot{\varepsilon}_d - 0.289 & For\ \dot{\varepsilon}_d > 63.1\ s^{-1} \end{cases} \quad (7)$$

c) In the 2008s, Zhou and Hao [74] proposed an equation to evaluate the DIF of concrete- like materials as follows:

$$DIF_{Zhou\ \&\ Hao} = \begin{cases} 0.0225\, log\, \dot{\varepsilon}_d + 1.12 & For\ \dot{\varepsilon}_d \le 10\ s^{-1} \\ 0.2713\ (log\, \dot{\varepsilon}_d)^2 - 0.3563 \log \dot{\varepsilon}_d + 1.2275 & For\ \dot{\varepsilon}_d > 10\ s^{-1} \end{cases} \quad (8)$$

In the present study, the dynamic increase factor curves of the experimental test were extended behind the strain rate of 30 s^{-1} until the static condition when the DIF is equal to 1. The experimental dynamic increase factors of both concrete types under temperatures of 25, 400, and 700 ^oC were compared with the results of the recommended expressions of dynamic increase factor as described in Fig. 6. The outcomes proved that the CEB model expression may efficiently estimate the dynamic increase factor of both concrete types under room temperature. However, the differences between the experimental and CEB results clearly increased at elevated temperatures particularly in case of PC under 400 and 700 ^oC that may attribute to the great loss in concrete strength. Nevertheless, the CEB model was more reliable to predict the behaviour of HVFANS concrete under mentioned temperatures that reflect the excellent role of nanosilica material which significantly enhances the strength of concrete under high temperature.

It can be concluded that the CEB expression could successfully use to obtain a full range of dynamic increase factor versus strain rate relationship for HVFANS concrete in compression under temperatures of 25, 400, and 700 ^oC which could significantly utilize as input data for the nonlinear concrete material model in numerical analysis of structure constructed by using this type of concrete and subjected to fire and blast loads.

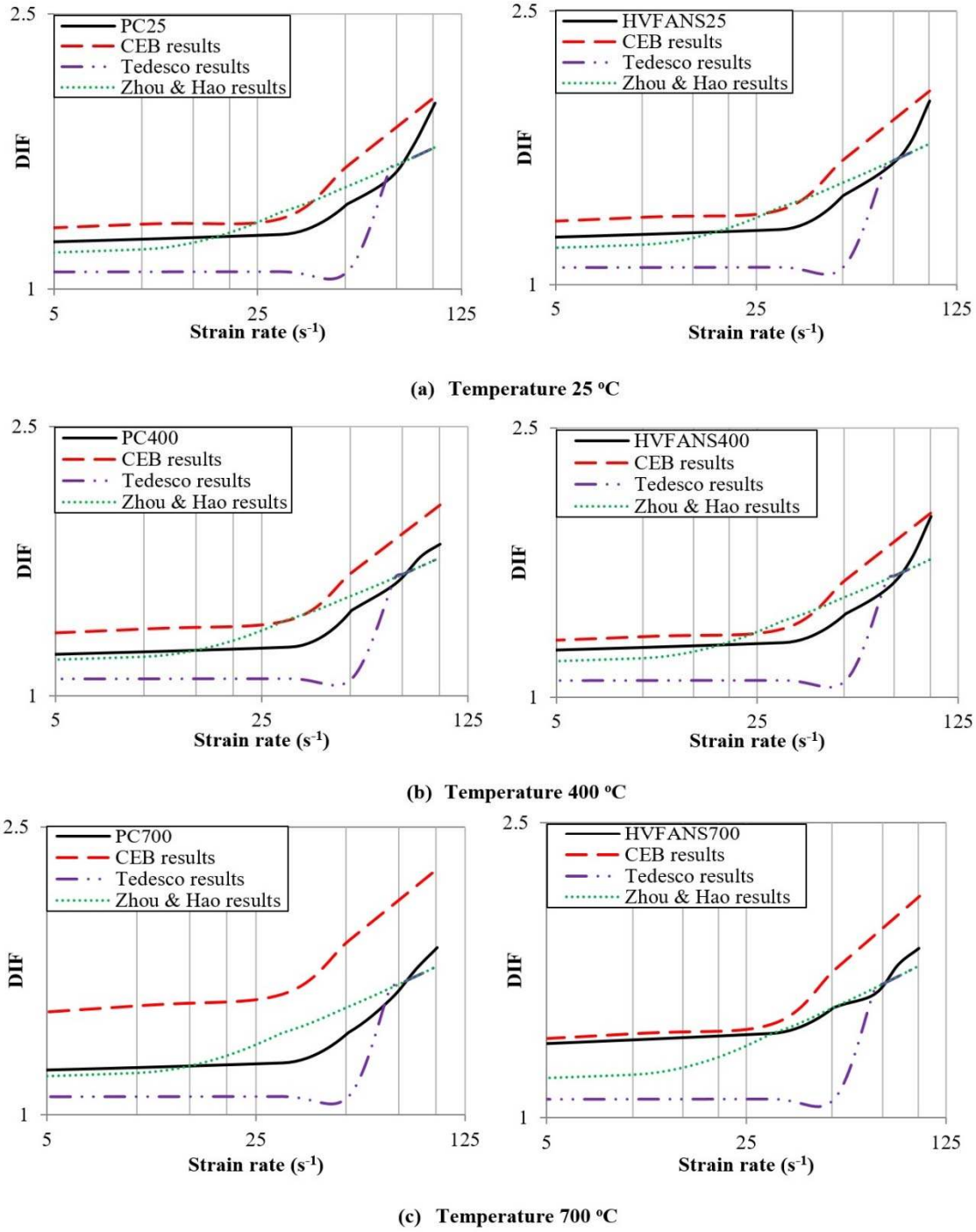


Fig. 6. *Comparison between DIF of test results and existing expressions at different temperatures*

3.2.2 Toughness

Specific energy absorption (SEA) defines as the energy absorption per unit volume of concrete material. Scholars used the SEA to characterize the toughness of concrete specimens as follows [3, 75, 76]:

$$SEA = \frac{AEc}{A_s l_s} \int_0^T \left[\varepsilon_i^2(t) - \varepsilon_r^2(t) - \varepsilon_t^2(t) \right] dt \qquad (9)$$

where A, E, c are the cross sectional area, Young's modulus, and elastic wave speed of bars, respectively, and l_s, A_s are the length and cross sectional area of the specimen: ε_i, ε_r, ε_t are the incident pulse, reflect pulse and transmit pulse, respectively; T is the complete failure moment of specimen. Figure 7 indicated that the SEA of PC and HVFANS

concrete specimens increased linearly with increasing of strain rate, similar behaviour was observed by researchers on concrete material tested by using SHPB machine under room or elevated temperatures [76, 77]. Small variances were noted in toughness of both concrete types at room temperature. However, the increase of temperature until 400 °C led to reducing the toughness of PC, while the same temperature caused an increase in toughness of HVFANS concrete by 9.79% under average strain rate of 100.67 s^{-1} as compared with the toughness at room temperature.

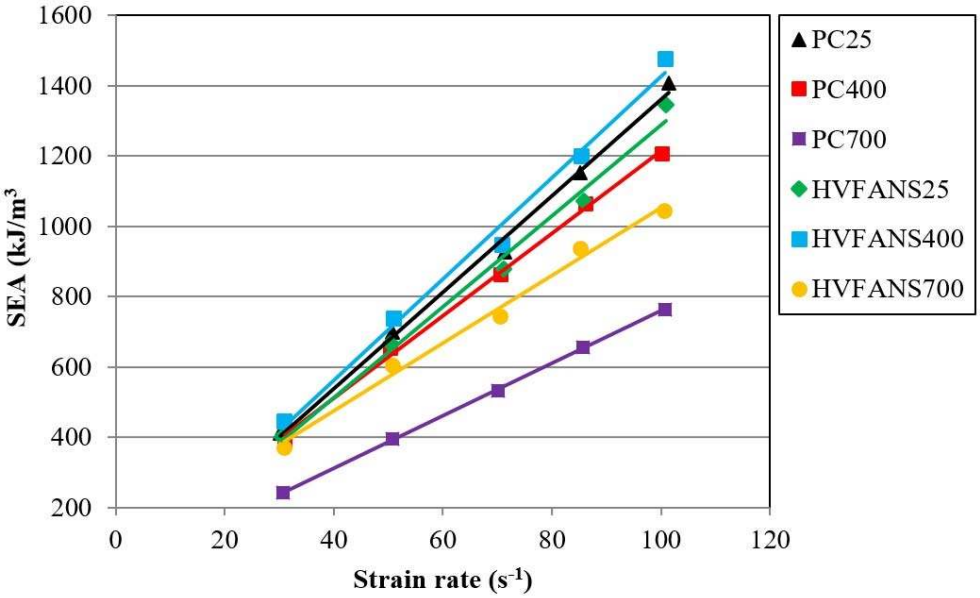


Fig. 7. *The toughness of PC and HVFANS concrete at various strain rates and temperatures.*

On the other hand, a notable reduction was observed in the toughness of PC and HVFANS at a temperature of 700 °C by 84.02 and 28.83% under average strain rates of 100.81 and 100.54 s^{-1}, respectively, as compared with the toughness at room temperature. Design Expert software was used to suggest the relationship of SEA with dynamic strain rate ($\dot{\varepsilon_d}$) and exposing temperature (T) by using quadratic solver model with square root and natural algorithm transformations for PC and HVFANS concrete, respectively, with a high accuracy as shown in Table 6.

For PC:

$$Sqrt\ (SEA) = 10.28522 + 0.013370\ T + \ 0.343809\ \dot{\varepsilon_d} - 0.000096\ T * \dot{\varepsilon_d} - 0.000025\ T^2 - 0.000769\ \dot{\varepsilon_d}^{\,2} \quad (10)$$

For HVFANS concrete:

$$\ln(SEA) = \ 5.13192 + 0.001126\ T + \ 0.030767\dot{\varepsilon_d} - \ 2.86175 * 10^{-6} * T * \dot{\varepsilon_d} - \ 1.57476 * 10^{-6} * T^2 - \ 0.000105\ \dot{\varepsilon_d}^{\,2} \quad (11)$$

where: T is the exposing temperature between 25 to 700 °C, and $\dot{\varepsilon_d}$ is the dynamic strain rate within a range of 30.12 to 101.42 s^{-1}.

Table 6. *The results of ANOVA analysis for SEA models of PC and HVFANS concrete*

Concrete	Transformation	Model	R^2	Adjusted R^2	Predicted R^2	Adequate Precision (AP)
PC	Square root	quadratic	0.9972	0.9956	0.9924	82.4900
HVFANS	Natural Log	quadratic	0.9910	0.9861	0.9774	41.0776

3.2.3 Critical strain

Critical strain defined as the strain of concrete corresponding to peak stress, which used to describe the ductility of PC and HVFANS concrete samples exposed to high strain rates and temperatures of 25, 400, and 700 °C

as shown in Fig. 8. The critical strain increased approximately linearly with increasing of strain rate and recorded small values at temperatures of 25 and 400 °C for both types of concrete ranged between 0.005 to 0.0075 due to the existent of PP fibres which considerably enhance the ductility of concrete and provide escape channels for vapour pressure inside the voids at elevated temperatures [78-80].

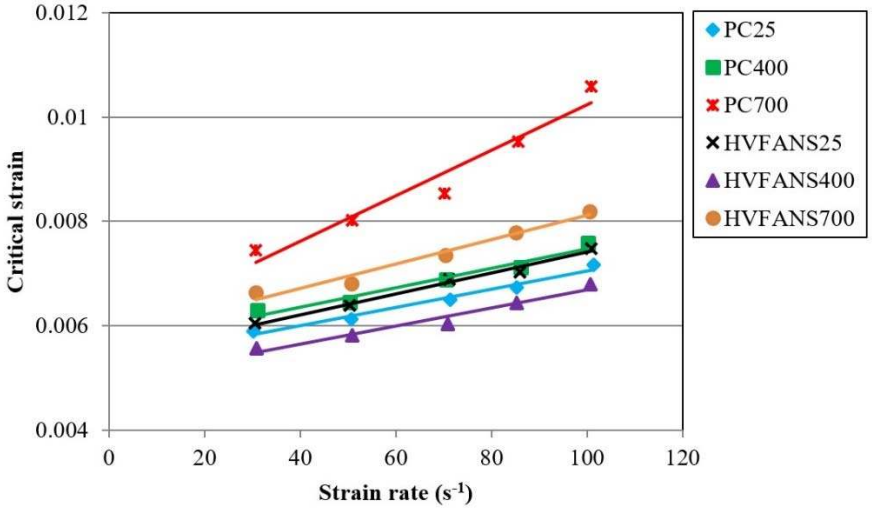


Fig. 8. *Critical strain of PC and HVFANS concrete at various strain rates and temperatures.*

The smallest values of critical strain were observed for HVFANS400 that may attribute to the high reactivity of NS in the mixture which increased at a heating temperature of 400 °C. Otherwise, the critical strain obviously increased at a temperature of 700 °C for both concrete types and the highest increment of critical strain was noted for PC700 by 47.75% as compared with PC25 under average strain rate of 100.81 s^{-1}. The relationship of critical strain (ε_{cr}) with dynamic strain rate ($\dot{\varepsilon}_d$) and temperature (T) was proposed by using Design Expert software with a quadratic solver model and inverse transformation for both concrete types within a good accuracy as shown in Table 7.

For PC:

$$\frac{1}{\varepsilon_{cr}} = 171.21120 + 0.040541\mathrm{T} - 0.055351\dot{\varepsilon_d} - 0.000199\,\mathrm{T} * \dot{\varepsilon_d} - 0.000119\,T^2 - 0.002501{\dot{\varepsilon_d}}^2 \quad (12)$$

For HVFANS concrete:

$$\frac{1}{\varepsilon_{cr}} = 170.76193 + 0.122916\,\mathrm{T} - 0.256219\dot{\varepsilon_d} - 0.000015\,\mathrm{T} * \dot{\varepsilon_d} - 0.000196\,T^2 - 0.001491{\dot{\varepsilon_d}}^2 \quad (13)$$

where: T is the exposing temperature between 25 to 700 °C, and $\dot{\varepsilon}_d$ is the dynamic strain rate within a range of 30.12 to 101.42 s^{-1}.

Table 7. *The results of ANOVA analysis for ε_{cr} models of PC and HVFANS concrete*

Concrete	Transformation	Model	R^2	Adjusted R^2	Predicted R^2	Adequate Precision (AP)
PC	inverse	quadratic	0.9949	0.9920	0.9811	59.4065
HVFANS	inverse	quadratic	0.9919	0.9874	0.9760	50.2862

3.2.4 Critical damage and Failure modes

Several studies had used the continuous damage mechanics theory to describe the critical damage of concrete under dynamic loads according to the differences in stress-strain curves with the increase of strain rate [81-83]. The critical damage variable (D_{cr}) was presented and defined as a scalar:

$$D_{cr} = \begin{cases} 0 & For\ \varepsilon_d = 0 \\ 1 - \dfrac{\sigma_p}{E_o \varepsilon_{cr}} & For\ \varepsilon_d > 0 \end{cases} \quad (14)$$

where σ_p is the peak stress, ε_{cr} is the critical strain and E_o is the initial modulus of elasticity. The given expression defined the critical damage as a kinematic variable that mainly relies on the density of voids or cracks in a specific cross section which may result in the gradual damage of concrete [84, 85]. The case of $D_{cr} = 1$ means that the concrete is not able to resist the applying loads. Figure 9 indicated that the critical damage increased almost linearly with the increase of strain rate and proved that the damage of HVFANS concrete at room temperature was slightly higher than PC under similar conditions of strain rate, that may attribute to the high volume of fly ash in the mixture. However, the HVFANS concrete appeared lower values of critical damage at temperatures of 400 and 700 ^{o}C by 6.26 and 9.14% under average strain rates of 100.67 and 100.54 s^{-1}, respectively, as compared with PC under similar range of strain rate.

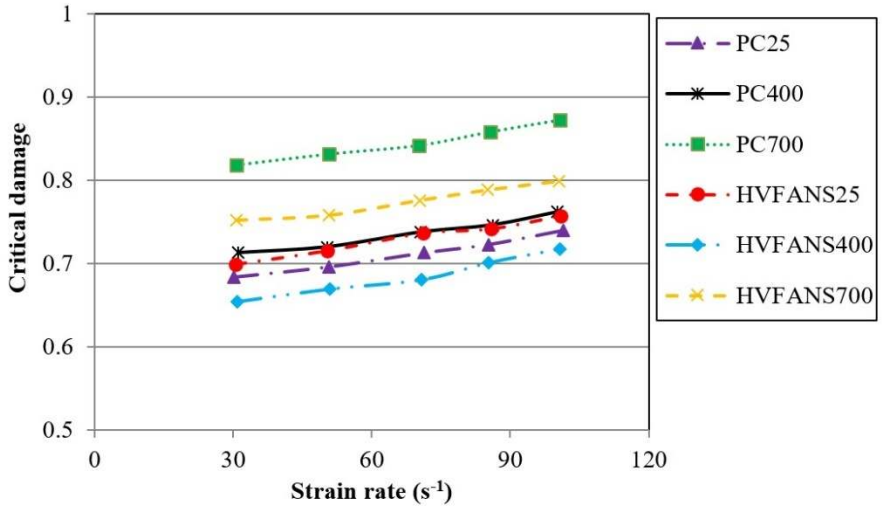


Fig. 9. *Critical damage of PC and HVFANS concrete at various strain rates and temperatures.*

During experimental study, the influences of strain rate and temperature on the damage of PC and HVFANS concrete were visible. The failure of concrete samples was so violent and caused severe destruction of cylindrical test samples into small pieces at high strain rates as shown in Fig. 10a. The pattern of shear failure could only observe at the range of strain rate between 30.12 to 70.91 s^{-1} under studied cases of room and elevated temperatures except for the case of PC under 700 ^{o}C which was totally destructed at an average strain rate of 70.17 s^{-1}. The variation of concrete failure with increasing of strain rates was shown in Fig.10b.

It can be noted that the shear failure of concrete samples could pass through three stages according to the increase of strain rate. In the first stage when the average strain rate between 30.12 to 50.91 s^{-1}, the crack's path was passed throughout the concrete mortar only. For average strain rates of 70.17 to 71.32 s^{-1}, the path of cracks was more straight and passed through a rough fracture surface which had a more broken aggregate that may attribute to the rapid increase of stress in samples which was quite sufficient to break the aggregate and concrete mortar zones along the path of less resistance. In the final stage of strain rates ($\geq$ 85.17 s^{-1}), the cracks amount was greatly increased and resulted in a severe fracturing of concrete samples into small fragments to dissipate the internal energy. In the same context, numerous researchers were obtained similar patterns of shear failure for cement-based materials according to the increase of strain rate [75, 86-88].

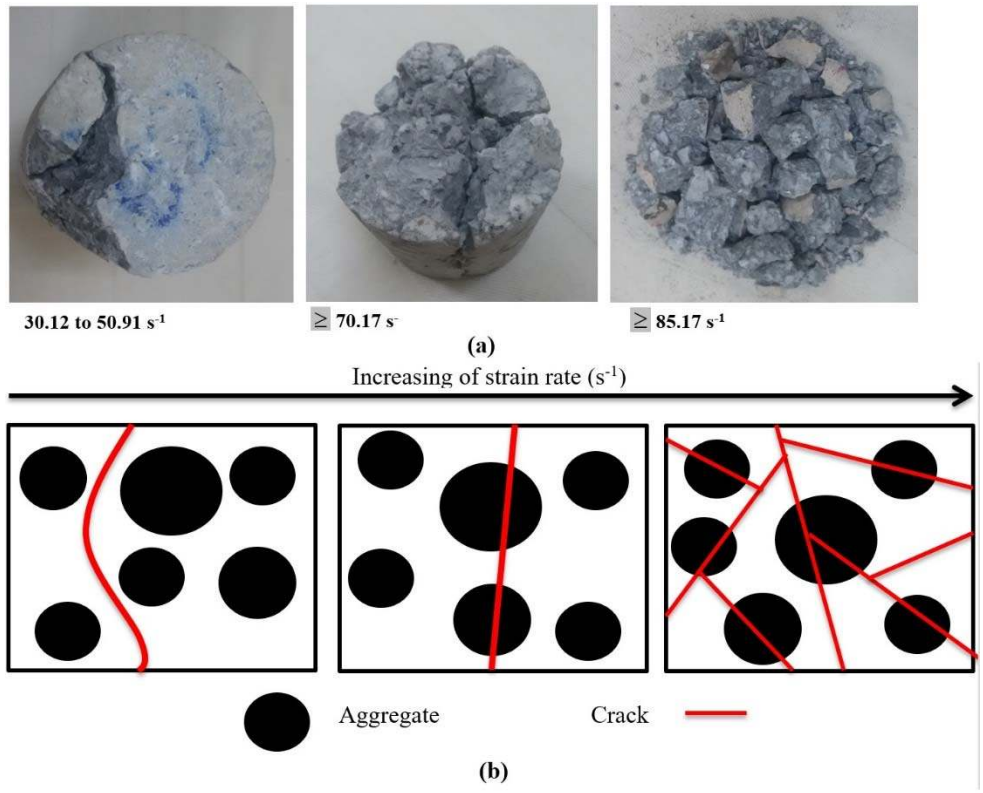


Fig. 10. *Failure modes of PC and HVFANS concrete at various strain rates.*

4. CONCLUSION

The results can be summarized as follows:

1. The static compressive strength of PC was higher by 4.21% than HVFANS concrete at room temperature. A dramatic reduction in compressive strength was observed at 700 ^{o}C for both types of concrete; nevertheless, the HVFANS concrete recorded a high residual strength of 85.13% as compared with PC which maintained 59.44%.
2. HVFANS concrete achieved an excellent performance than PC in terms of dynamic compressive strength, toughness, critical strain and damage under elevated temperatures of 400 and 700 ^{o}C subjected to average strain rate between 30.12 to 101.42 s^{-1}.
3. The CEB model was the most appropriate to predict the dynamic increase factors of HVFANS concrete under the studied temperatures.
4. Equations were proposed to predict the dynamic increase factor, toughness, and critical strain of both concretes within an exposing temperature range of 25 to 700 ^{o}C and average strain rate of 30.12 to 101.42 s^{-1}.

The mentioned results proved a good possibility to use HVFANS concrete in structures to improve its resistant to fire and dynamic loads, besides its eco-friendly properties.

Acknowledgments

The authors would like to acknowledge the financial support from the Fundamental Research Grant Scheme (grant number FRGS/1/2015/ TK01/UKM/02/4), Arus Perdana Grant (AP-2015-011) and Dana Impak Perdana (grant number DIP-2014-019) to perform this research.

References

1. Khoury, G.A., B.N. Grainger, and P.J. Sullivan, *Strain of concrete during first heating to 600 C under load*. Magazine of concrete research, 1985. **37**(133): p. 195-215.

2. Malhotra, H., *The effect of temperature on the compressive strength of concrete*. Magazine of concrete research, 1956. **8**(23): p. 85-94.

3. Li, Z., J. Xu, and E. Bai, *Static and dynamic mechanical properties of concrete after high temperature exposure*. Materials Science and Engineering: A, 2012. **544**: p. 27-32.

4. Buchanan, A.H. and A.K. Abu, *Structural design for fire safety*. 2017: John Wiley & Sons.

5. Lamond, J.F., *Significance of tests and properties of concrete and concrete-making materials*. Vol. 169. 2006: ASTM International.

6. Ibrahim, R.K., et al., *The effect of high temperature on mortars containing silica fume*. Journal of Applied Sciences, 2011. **11**(14): p. 2666-2669.

7. Behnood, A. and H. Ziari, *Effects of silica fume addition and water to cement ratio on the properties of high-strength concrete after exposure to high temperatures*. Cement and Concrete Composites, 2008. **30**(2): p. 106-112.

8. Flower, D.J. and J.G. Sanjayan, *Green house gas emissions due to concrete manufacture*. The international Journal of life cycle assessment, 2007. **12**(5): p. 282.

9. Bouzoubaa, N., et al., *Laboratory-produced high-volume fly ash blended cements: physical properties and compressive strength of mortars*. Cement and Concrete Research, 1998. **28**(11): p. 1555-1569.

10. Sivasundaram, V., G. Carette, and V. Malhotra, *Selected properties of high-volume fly ash concretes*. Concrete International, 1990. **12**(10): p. 47-50.

11. McCarthy, M. and R. Dhir, *Development of high volume fly ash cements for use in concrete construction*. Fuel, 2005. **84**(11): p. 1423-1432.

12. C311, A., *Standard Test Methods for Sampling and Testing Fly Ash or Natural Pozzolans for Use as a Mineral Admixture in Portland-Cement Concrete*. 2000, ASTM International West Conshohocken, Pa.

13. Dunstan, M., et al., *Investigation into the long-term in-situ performance of high fly ash content concrete used for structural applications.* Special Publication, 1992. **132**: p. 1-20.

14. Bilodeau, A. and V. MalhotraI, *Concretes Incorporating High Volumes of ASTM Class F Fly Ashes: Mechanical Properties and Resistance to De-icing Salt Scaling and to Chloride-Ion Penetration.* Special Publication, 1992. **132**: p. 319-350.

15. Burke, D. *Development of Concrete Mixtures with High-Volume Fly Ash Cement Replacement*. in *2012 International Concrete Sustainability Conference, National Ready Mixed Concrete Association*. 2012.

16. Burden, D., *The durability of concrete containing high levels of fly ash*. 2006, University of New Brunswick, Department of Civil Engineering.

17. Şahmaran, M., et al., *Self-healing of mechanically-loaded self consolidating concretes with high volumes of fly ash*. Cement and Concrete Composites, 2008. **30**(10): p. 872-879.

18. Younsi, A., et al., *Performance-based design and carbonation of concrete with high fly ash content.* Cement and Concrete Composites, 2011. **33**(10): p. 993-1000.

19. Bentz, D.P. and C.F. Ferraris, *Rheology and setting of high volume fly ash mixtures*. Cement and Concrete Composites, 2010. **32**(4): p. 265-270.

20. Şahmaran, M., İ.Ö. Yaman, and M. Tokyay, *Transport and mechanical properties of self consolidating concrete with high volume fly ash*. Cement and concrete composites, 2009. **31**(2): p. 99-106.

21. Qing, Y., et al., *Influence of nano-SiO 2 addition on properties of hardened cement paste as compared with silica fume*. Construction and Building Materials, 2007. **21**(3): p. 539-545.

22. Jo, B.-W., et al., *Characteristics of cement mortar with nano-SiO 2 particles*. Construction and building materials, 2007. **21**(6): p. 1351-1355.

23. Collepardi, M., et al. *Optimization of silica fume, fly ash and amorphous nano-silica in superplasticized high-performance concretes*. in *Proceedings of 8th CANMET/ACI International Conference on Fly Ash, Silica Fume, Slag and Natural Pozzolans in Concrete, SP-221, Las Vegas, USA*. 2004.

24. Zhang, M.-H. and J. Islam, *Use of nano-silica to reduce setting time and increase early strength of concretes with high volumes of fly ash or slag*. Construction and Building Materials, 2012. **29**: p. 573-580.

25. Ibrahim, R.K., *The strength and micro structures of sustainable high strength high-volume fly ash concrete with nano materials exposed to high temperature, Ph.D. thesis.*, in *Department of Civil and Structural Engineering*. 2013, Universiti Kebangsaan Malaysia (UKM): Malaysia.

26. Ibrahim, R.K., R. Hamid, and M.R. Taha, *Fire resistance of high-volume fly ash mortars with nanosilica addition*. Construction and Building Materials, 2012. **36**: p. 779-786.

27. Radzi, N.A.M., *Behaviour of a High Strength High-Volume Fly Ash Nano-Silica RC Slab under ISO 834 Fire Curve Exposure, M.Sc. thesis*, in *Department of Civil and Structural Engineering*. 2016, Universiti Kebangsaan Malaysia (UKM): Malaysia.

28. Mussa, M.H., et al., *Assessment of damage to an underground box tunnel by a surface explosion*. Tunnelling and Underground Space Technology, 2017. **66**: p. 64-76.

29. Mutalib, A.A. and H. Hao, *Development of PI diagrams for FRP strengthened RC columns*. International journal of impact engineering, 2011. **38**(5): p. 290-304.

30. Lu, Y., et al., *Dynamic compressive behavior of recycled aggregate concrete based on split Hopkinson pressure bar tests*. Latin American Journal of Solids and Structures, 2014. **11**(1): p. 131-141.

31. Cai, Y., S. Yu, and Y. Lu, *Experimental study on granite and the determination of its true strain-rate effect*. Latin American Journal of Solids and Structures, 2015. **12**(4): p. 675-694.

32. Huo, J., et al., *Experimental study on dynamic behaviours of concrete after exposure to high temperatures up to 700 C*. Materials and structures, 2013. **46**(1-2): p. 255-265.

33. Ziyan, L.C.L.Y.W. and G.W.G. Yuzhuo, *Dynamic compression behavior of heated concrete*. China Civil Engineering Journal, 2011. **4**: p. 013.

34. He, Y., J. Huo, and Y. Xiao, *Experimental study on dynamic behavior of concrete at elevated temperatures*. Advanced Science Letters, 2011. **4**(3): p. 1128-1131.

35. Su, H., J. Xu, and W. Ren, *Experimental study on the dynamic compressive mechanical properties of concrete at elevated temperature*. Materials & Design, 2014. **56**: p. 579-588.

36. Chen, L., et al., *Combined effects of high temperature and high strain rate on normal weight concrete*. International Journal of Impact Engineering, 2015. **86**: p. 40-56.

37. Zhai, C., et al., *Experimental study of strain rate effects on normal weight concrete after exposure to elevated temperature*. Materials and Structures, 2017. **50**(1): p. 40.

38. Standard, M., *Portland cement (ordinary and rapid-hardening): Part 1.* Specification (Second revision), Malaysia, MS, 2003. **522**.

39. STANDARD, B., *Fly ash for concrete*—. 2005, Part.

40. Standard, A., *C136, 2006,".* Standard Test Method for Sieve Analysis of Fine and Coarse Aggregates," ASTM International, West Conshohocken, PA, 2006.

41. ASTM, A., *C128-07a Standard Test Method for Density, Relative Density (Specific Gravity), and Absorption of Fine Aggregate.* 2007. ASTM International: West Conshohocken, PA.

42. ASTM, C., *29, Standard test method for bulk density (" Unit Weight") and voids in aggregate.* American Society for Testing and Materials, Annual Book, Pennsylvania, USA, 2009.

43. Banthia, N. and R. Gupta, *Influence of polypropylene fiber geometry on plastic shrinkage cracking in concrete*. Cement and Concrete Research, 2006. **36**(7): p. 1263-1267.

44. Qian, C. and P. Stroeven, *Development of hybrid polypropylene-steel fibre-reinforced concrete*. Cement and Concrete Research, 2000. **30**(1): p. 63-69.

45. Alhozaimy, A., P. Soroushian, and F. Mirza, *Mechanical properties of polypropylene fiber reinforced concrete and the effects of pozzolanic materials*. Cement and Concrete Composites, 1996. **18**(2): p. 85-92.

46. Toutanji, H.A., *Properties of polypropylene fiber reinforced silica fume expansive-cement concrete*. Construction and Building Materials, 1999. **13**(4): p. 171-177.

47. Kalifa, P., G. Chene, and C. Galle, *High-temperature behaviour of HPC with polypropylene fibres: From spalling to microstructure*. Cement and concrete research, 2001. **31**(10): p. 1487-1499.

48. Committee211, A., *Guide for selecting proportions for high-strength concrete with portland cement & fly ash-ACI 211.4 R-93*. 1998, Farming-ton Hills, Michigan: American Concrete Institute.

49. Standard, A., *C192. 2007.* Standard Practice for Making and Curing Concrete Test Specimens in the Laboratory (ASTM C192-07). West Conshohocken, PA: ASTM International.

50. Neville, A.M., *Properties of concrete.* 1995.

51. Standard, M.J., *Thermal Insulation - Determination of Steady-state Thermal Resistance and Related Properties - Guarded Hot Plate Apparatus (ISO 8302: 1991, IDT)*. 2003: Department of Standards Malaysia.

52. EN, B., *12390-3. Testing hardened concrete*. Compressive strength of test specimens, 2009. **19**.

53. Al-Masoodi, A.H.H., et al., *Static and dynamic properties of concrete with different types and shapes of fibrous reinforcement*. Construction and Building Materials, 2016. **104**: p. 247-262.

54. Chien Yet, T., R. Hamid, and M. Kasmuri, *Dynamic stress-strain behaviour of steel fiber reinforced high-performance concrete with fly ash*. Advances in Civil Engineering, 2012. **2012**.

55. Lindholm, U.S., *High strain rate tests*. Measurement of mechanical properties, 1971. **5**(Part 1): p. 199-271.

56. Bertholf, L. and C. Karnes, *Two-dimensional analysis of the split Hopkinson pressure bar system*. Journal of the Mechanics and Physics of Solids, 1975. **23**(1): p. 1-19.

57. Davies, E. and S. Hunter, *The dynamic compression testing of solids by the method of the split Hopkinson pressure bar*. Journal of the Mechanics and Physics of Solids, 1963. **11**(3): p. 155-179.

58. Kirby, M.S.P., *Designing a Data Acquisition System for a Split Hopkinson Pressure Bar*.

59. Dyab, M.M., *Providing Learning Opportunities by Designing a Split Hopkinson Pressure Bar*. age, 2013. **23**: p. 1.

60. Li, J. and Y. Zhang, *Evaluation of constitutive models of hybrid-fibre engineered cementitious composites under dynamic loadings*. Construction and Building Materials, 2012. **30**: p. 149-160.

61. Jawed, I., et al., *High-strain-rate behavior of hydrated cement pastes*. Cement and Concrete Research, 1987. **17**(3): p. 433-440.

62. Lok, T., P. Zhao, and G. Lu, *Using the split Hopkinson pressure bar to investigate the dynamic behaviour of SFRC*. Magazine of Concrete Research, 2003. **55**(2): p. 183-191.

63. Lu, Y. and Q. Li, *Appraisal of pulse-shaping technique in split Hopkinson pressure bar tests for brittle materials*. International Journal of Protective Structures, 2010. **1**(3): p. 363-390.

64. Berndt, M., *Properties of sustainable concrete containing fly ash, slag and recycled concrete aggregate*. Construction and building materials, 2009. **23**(7): p. 2606-2613.

65. Miller, O., L. Freund, and A. Needleman, *Modeling and simulation of dynamic fragmentation in brittle materials*. International Journal of Fracture, 1999. **96**(2): p. 101-125.

66. Vaughn, N. and C. Polnaszek, *Design-Expert® software*. Stat-Ease, Inc, Minneapolis, MN, 2007.

67. Joglekar, A. and A. May, *Product excellence through design of experiments*. Cereal foods world, 1987. **32**(12): p. 857-&.

68. Noordin, M.Y., et al., *Application of response surface methodology in describing the performance of coated carbide tools when turning AISI 1045 steel*. Journal of materials processing technology, 2004. **145**(1): p. 46-58.

69. Montgomery, D.C., *Design and Analysis of Experiments* 6th Edition with Design Expert Software. 2004: John Wiley & Sons.

70. Malvar, L.J. and C.A. Ross, *Review of strain rate effects for concrete in tension*. Materials Journal, 1998. **95**(6): p. 735-739.

71. Bischoff, P. and S. Perry, *Compressive behaviour of concrete at high strain rates*. Materials and structures, 1991. **24**(6): p. 425-450.

72. MC90, C., *Design of Concrete Structures. CEB-FIP Model Code 1990*. 1993, Thomas Telford.

73. Tedesco, J., et al., *A strain-rate-dependent concrete material model for ADINA*. Computers & structures, 1997. **64**(5-6): p. 1053-1067.

74. Zhou, X. and H. Hao, *Modelling of compressive behaviour of concrete-like materials at high strain rate*. International Journal of Solids and Structures, 2008. **45**(17): p. 4648-4661.

75. Li, W. and J. Xu, *Mechanical properties of basalt fiber reinforced geopolymeric concrete under impact loading*. Materials Science and Engineering: A, 2009. **505**(1): p. 178-186.

76. Li, W. and J. Xu, *Impact characterization of basalt fiber reinforced geopolymeric concrete using a 100-mm-diameter split Hopkinson pressure bar*. Materials Science and Engineering: A, 2009. **513**: p. 145-153.

77. Wang, S., M.-H. Zhang, and S.T. Quek, *Effect of specimen size on static strength and dynamic increase factor of high-strength concrete from SHPB test*. Journal of Testing and Evaluation, 2011. **39**(5): p. 1-10.

78. Köksal, F., et al., *Combined effect of silica fume and steel fiber on the mechanical properties of high strength concretes*. Construction and Building Materials, 2008. **22**(8): p. 1874-1880.

79. Shannag, M., *High strength concrete containing natural pozzolan and silica fume*. Cement and concrete composites, 2000. **22**(6): p. 399-406.

80. Nili, M. and V. Afroughsabet, *The effects of silica fume and polypropylene fibers on the impact resistance and mechanical properties of concrete*. Construction and Building Materials, 2010. **24**(6): p. 927-933.

81. Clayton, J.D., *A model for deformation and fragmentation in crushable brittle solids*. International Journal of Impact Engineering, 2008. **35**(5): p. 269-289.

82. Wang, Z.-L., Y.-S. Liu, and R. Shen, *Stress–strain relationship of steel fiber-reinforced concrete under dynamic compression*. Construction and Building Materials, 2008. **22**(5): p. 811-819.

83. Hamdi, E., N.B. Romdhane, and J.-M. Le Cléac'h, *A tensile damage model for rocks: application to blast induced damage assessment*. Computers and Geotechnics, 2011. **38**(2): p. 133-141.

84. Addessio, F.L. and J.N. Johnson, *A constitutive model for the dynamic response of brittle materials*. Journal of Applied Physics, 1990. **67**(7): p. 3275-3286.

85. Wang, Z.-l., Y.-c. Li, and J. Wang, *A damage-softening statistical constitutive model considering rock residual strength*. Computers & Geosciences, 2007. **33**(1): p. 1-9.

86. Wu, W., W. Zhang, and G. Ma, *Mechanical properties of copper slag reinforced concrete under dynamic compression*. Construction and Building Materials, 2010. **24**(6): p. 910-917.

87. Wang, S., M.-H. Zhang, and S.T. Quek, *Mechanical behavior of fiber-reinforced high-strength concrete subjected to high strain-rate compressive loading*. Construction and Building Materials, 2012. **31**: p. 1-11.

88. Liu, F., et al., *Study of impact performance of rubber reinforced concrete*. Construction and Building Materials, 2012. **36**: p. 604-616.